Supplementary Material: QuinNet: Efficiently Incorporating Quintuple Interactions into Geometric Deep Learning force Fields

Zun Wang
Microsoft Research AI4Science
Beijing, China, 100084
zunwang@microsoft.com

Guoqing Liu
Microsoft Research AI4Science
Beijing, China, 100084

Yichi Zhou
Microsoft Research AI4Science
Beijing, China, 100084

Tong Wang
Microsoft Research AI4Science
Beijing, China, 100084

Bin Shao
Microsoft Research AI4Science
Beijing, China, 100084
binshao@microsoft.com

1 Supplementary Material

1.1 Proof of equivariance

As all the many-body interactions in the QuinNet are calculated based on inner product and cross product, the proof for the equivariance of these modules is equivalent to prove the equivariance of inner product and cross product. Let $\mathbf{R}$ be a 3×3 rotation matrix, i.e. $\det \mathbf{R} = 1$ and $\mathbf{R}^{-1} = \mathbf{R}^T$, for all vectors $\vec{u}, \vec{v} \in \mathbb{R}^3$,

$$\begin{aligned}(\mathbf{R}\vec{u}) \cdot (\mathbf{R}\vec{v}) &= (\mathbf{R}\vec{u})_i (\mathbf{R}\vec{v})_i \\ &= R_{ij} u_j R_{ik} v_k \\ &= R_{ij} R_{ik} u_j v_k \\ &= (\mathbf{R}^T)_{ji} \mathbf{R}_{ik} u_j v_k \\ &= (\mathbf{R}^T \mathbf{R})_{jk} u_j v_k \\ &= \delta_{jk} u_j v_k \\ &= u_j v_j \\ &= \vec{u} \cdot \vec{v},\end{aligned} \tag{1}$$

37th Conference on Neural Information Processing Systems (NeurIPS 2023).

Table S 1: Comparison of the MAEs on Chignolin dataset and the lowest values are marked in bold (energies in kcal/mol and forces in kcal/(mol·Å)).

		ViSNet-LSRM	3-body (ET)	4-body (ViSNet)	4-body (improper)	5-body@I	5-body@II	5-body (QuinNet)	QuinNet (6 Layer)
Chignolin	Energy	1.227	1.711± 0.012	1.296± 0.044	1.234± 0.036	1.317± 0.042	1.241± 0.072	1.079± 0.019	**1.036**
	Force	0.2778	0.4014± 0.0015	0.2944± 0.0022	0.2944± 0.0039	0.2980± 0.0066	0.2922± 0.0073	0.2747± 0.0030	**0.2665**

where δ_{jk} is the Kronecker delta symbol and the Einstein summation convention is used. To prove the equivariance of cross product, the Levi-Civita permutation symbol ϵ would be used,

$$\begin{aligned}
[(\mathbf{R}\vec{u}) \times (\mathbf{R}\vec{v})]^k &= \epsilon^{imk} R_{ij} R_{mn} u^j v^n \\
&= \epsilon^{iml} \delta_{kl} R_{ij} R_{mn} u^j v^n \\
&= \epsilon^{iml} R_{kr} R_{lr} R_{ij} R_{mn} u^j v^n \\
&= \epsilon^{jnr} \det \mathbf{R} R_{kr} u^j v^n \\
&= R_{kr} \epsilon^{jnr} u^j v^n \\
&= R_{kr} (\vec{u} \times \vec{v})^r \\
&= \mathbf{R} \cdot (\vec{u} \times \vec{v})^k.
\end{aligned} \tag{2}$$

1.2 Proof of higher order cosine series

The Legendre polynomials could be expressed as

$$P_l(\cos\theta) = 2^l \sum_{k=0}^{l} \cos^k\theta \binom{l}{k} \binom{\frac{l+k-1}{2}}{l}. \tag{3}$$

Incorporating higher order cosine series into the QuinNet model is necessary in certain cases. These series can be represented as $\cos(n\theta)$ and can be expanded as a linear combination of $\cos^k\theta$ according to two-fold duplication formula, i.e. $\cos 2\theta = 2\cos^2\theta - 1$. Therefore, the vector addition theorem of spherical harmonic functions can be used to incorporate these higher order cosine series into the model.

1.3 Additional results on Chignolin

Table S 1 reports the MAEs of the benchmarked model, along with the results of the ablation study. It should be noted that in the ablation study, the benchmarked models, which includes only 3-body interactions, and incorporates 4-body interactions, are ET [1] and ViSNet [2] model respectively. Furthermore, the results of the 6-layer QuinNet model are presented in the table.

1.4 Results on QM9 dataset

The QM9 dataset [3, 4] encompasses computed geometric, energetic, electronic, and thermodynamic properties of 134k stable small organic molecules, which include carbon, hydrogen, oxygen, nitrogen, and fluorine, ascertained at the B3LYP/6-31G (2df, p) level of quantum chemistry. This dataset offers valuable quantum chemical insights into the chemical space of small organic molecules and is widely acknowledged as a benchmark for calibrating, analyzing, and evaluating new methods in this area. As a result, we trained QuinNet on 110k molecules and validated it on a further 10k molecules. Table 2 presents the mean absolute errors (MAEs) of QuinNet for 12 tasks in the QM9 dataset, compared to four other models. Despite the QM9 dataset being a small molecular dataset where the influence of five-body interactions is relatively weak, QuinNet's MAEs are in line with these baselines. It is worth noting that the gap is computed directly from the predicted HOMO and LUMO values.

1.5 Further Complexity Analysis

To further highlight the efficiency of the QuinNet model, Table S 3 presents a comparison of time complexities for handling many-body interactions between QuinNet and the empirical force field. In the table, N and N_b denote the number of atoms and the number of neighbors, respectively. Note that the number of atoms N is ignored in the complexity analysis of QuinNet. Additionally, we

Table S 2: Comparison of the MAEs on QM9 dataset and the lowest values are marked in bold.

	unit	Allegro [5]	Equiformer [6]	ViSNet [2]	QuinNet
μ	D	-	0.014	**0.010**	0.771
α	a_0^3	-	0.056	**0.041**	0.047
HOMO	meV	-	**17**	**17.3**	20.4
LUMO	meV	-	16	**14.8**	17.6
gap	meV	-	33	31.7	**28.2**
R^2	a_0^2	-	0.227	**0.030**	0.194
ZPVE	meV	-	1.32	1.56	**1.26**
U_0	meV	4.7	10	**4.23**	7.6
U	meV	4.4	11	**4.25**	8.4
H	meV	**4.4**	10	4.52	7.8
G	meV	**5.7**	10	5.86	8.5
C_v	$\frac{kcal}{mol \cdot K}$	-	0.025	**0.023**	0.024

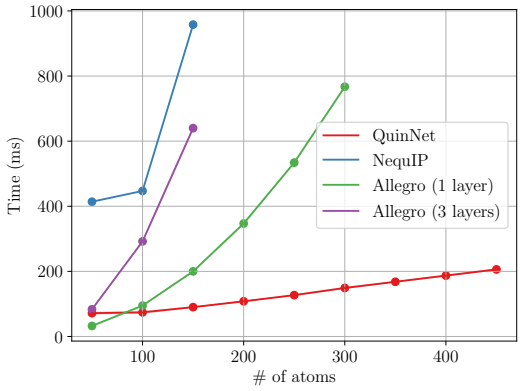

Fig. S 1: The inference time of different models with a single 32GB V100 GPU card.

evaluate the inference time of different models with a single 32GB V100 GPU card (Fig. S1). As the system size increases, the NequIP and Allgro models encounter out-of-memory issues. In general, the inference time of QuinNet is lower compared to the other benchmarked models.

1.6 Overlap between many-body interactions

The QuinNet model is designed to effectively capture all possible five-body interactions, which have some overlaps with other many-body interactions actually. Specifically, as shown in Fig. S2 (a), we illustrate the topology of five-body@I interactions, which includes four neighboring nodes, namely j_1, j_2, j_3, and j_4, with respect to the central node i. However, when $j_2 = j_4$ (Fig. S2 (b)), the topology reduces to a four-body interaction similar to an improper torsion interaction. Through this transformation, the five-body@I term characterizes the improper term associated with dihedral angles. The QuinNet model captures all five-body interactions, making it a versatile and comprehensive tool for modeling complex molecular systems.

1.7 Settings of experiments

The loss function for training QuinNet model is the weighted summation of mean square errors of energy and forces,

$$L = \alpha L_E + \beta L_F = \frac{\alpha}{N} \sum_{i}^{N} (E_i - \hat{E}_i)^2 + \frac{\beta}{3N_a} \sum_{\substack{i, \\ \sigma=x,y,z}}^{N_a} (F_{i\sigma} - \hat{F}_{i\sigma})^2, \tag{4}$$

where N and N_a are batch size and the number of atoms, respectively. AdamW optimizer [7] was adopted. QuinNet model was trained on 32G Nvidia Tesla V100 GPUs for MD17, revised MD17

Table S 3: Comparison of time complexities for handling many-body interactions between QuinNet and the empirical force field.

N-body	Empirical force field	Pseudocode of QuinNet	Time Complexity	
			Empirical force field	QuinNet

3-body	For each atom i, choose two neighbor atoms j and k to calculate angles.	$m_i = 0$
		for $j \in \mathcal{N}_i$ **do**
		  $m_i += \vec{r}_{ij}$
		end for
		$h_i = m_i^2$
			$NC_{N_b}^2 \sim \mathcal{O}(NN_b^2)$	$\mathcal{O}(N_b)$

4-body (torsion)	For each atom i, choose two neighbor atoms j and k firstly, then choose one neighbor atom l of atom j to calculate dihedral angles.	$h_{ij,1}, h_{ij,2} = 0, 0$
		for $k_1 \in \mathcal{N}_i$ **do**
		  $h_{ij,1} += \vec{r}_{ik_1} \times \vec{r}_{ij}$
		end for
		for $k_2 \in \mathcal{N}_j$ **do**
		  $h_{ij,2} += -\vec{r}_{jk_2} \times \vec{r}_{ij}$
		end for
		$h_{ij} = h_{ij,1} \cdot h_{ij,2}$
			$NC_{N_b}^2 C_{N_b}^1 \sim \mathcal{O}(NN_b^3)$	$\mathcal{O}(N_b)$

4-body (improper)	For each atom i, choose three neighbor atoms j, k, and l to calculate angles.	$m_i, h_{i,1}, h_{i,2} = 0, 0, 0$
		for $j \in \mathcal{N}_i$ **do**
		  $m_i += \vec{r}_{ij}$
		  $h_{i,1} += \alpha_j \vec{r}_{ij}$
		  $h_{i,2} += \beta_j \vec{r}_{ij}$
		end for
		$h_i = m_i \cdot (h_{i,1} \times h_{i,2})$
			$NC_{N_b}^3 \sim \mathcal{O}(NN_b^3)$	$\mathcal{O}(N_b)$

5-body@I	For each atom i, choose four neighbor atoms j, k, l, and m to calculate dihedral angles.	$h_{i,1}, h_{i,2} = 0, 0$
		for $j \in \mathcal{N}_i$ **do**
		  $h_{i,1} += \alpha_j \vec{r}_{ij}$
		  $h_{i,2} += \beta_j \vec{r}_{ij}$
		end for
		$h_i = (h_{i,1} \times h_{i,2})^2$
			$NC_{N_b}^4 \sim \mathcal{O}(NN_b^4)$	$\mathcal{O}(N_b)$

5-body@II	For each atom i, choose two neighbor atoms j_1 and j_2, then choose one neighbor atom k for each atom j to calculate dihedral angles.	$h_{j,1}, h_{j,2}, h_i = 0, 0, 0$
		for $k \in \mathcal{N}_j$ **do**
		  $h_{j,1} += \alpha_k \vec{r}_{kj}$
		  $h_{j,2} += \beta_k \vec{r}_{ij}$
		end for
		for $j \in \mathcal{N}_i$ **do**
		  $h_i += h_{j,1} \times h_{j,2}$
		end for
		$h_i = h_i^2$
			$NC_{N_b}^2 C_{N_b}^1 C_{N_b}^1 \sim \mathcal{O}(NN_b^4)$	$\mathcal{O}(N_b)$

5-body@III	For each atom i, choose three neighbor atoms j_1, j_2, and j_3, then choose one neighbor atom k for one of the thee neighbor atoms of i to calculate dihedral angles.	$h_{j,1}, h_{j,2} = 0, 0$
		for $k \in \mathcal{N}_j$ **do**
		  $h_{j,1} += \alpha_k \vec{r}_{kj}$
		  $h_{j,2} += \beta_k \vec{r}_{kj}$
		end for
		$h_j = h_{j,1} \times h_{j,2}$
		for $j \in \mathcal{N}_i$ **do**
		  $h_{ij} += h_i \dot{h}_j$
		end for
			$NC_{N_b}^3 C_{N_b}^1 \sim \mathcal{O}(NN_b^4)$	$\mathcal{O}(N_b)$

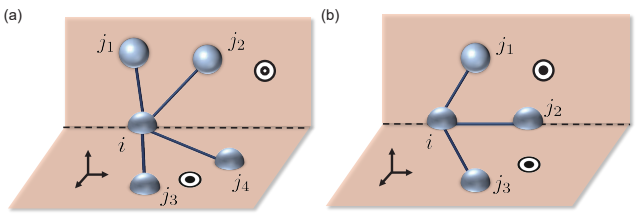

Fig. S 2: A comparison between five-body and many-body interactions. (a) five-body interactions@I, which involves four neighboring nodes, can overlap with (b) the improper term in four-body interactions, resulting in a four-body interaction topology.

Table S 4: Hyperparameters of QuinNet for different datasets.

	MD17	revised MD17	MD22	Chignolin	QM9
Energy/force weights	0.01, 0.99	0.01, 0.99	0.01, 0.99	0.01, 0.99	-
Energy/force ema	0.05, 1.0	0.05, 1.0	0.05, 1.0	0.05, 1.0	-
Cutoff (Å)	4.0, 5.0	4.0, 5.0	4.0, 5.0	5.0	5.0
# layers	5	5	5	5	5
# neurons	256	256	256	256	256
Batch size	4	2, 4	2, 4	8	16
Learning rate (LR)	2e-4, 4e-4	2e-4, 4e-4	2e-4, 4e-4	2e-4	2e-4, 3e-4, 4e-4, 5e-4
LR decay factors	0.8	0.8	0.8	0.8	0.8

and Chignolin dataset. For MD22 dataset, the model was trained on a single 80G Nvidia Tesla A100 GPU. Furthermore, detailed settings of hyperparameters are summarized in the Table S 4.

Moreover, to demonstrate QuinNet's performance, we performed molecular dynamics (MD) simulations of seven small molecules from the MD17 dataset. For each model and molecule, simulations began with the initial frame configurations and were performed over 300 ps. We employed a 0.5 fs time step and maintained the temperature at 500 K using a Nosé-Hoover thermostat. The distribution of interatomic distances, h(r), was calculated as the ensemble average of distance statistics within the trajectories. The code for the simulation was implemented using the ASE [8] Python package and adapted from Ref. [9].

References

[1] Philipp Thölke and Gianni De Fabritiis. Equivariant transformers for neural network based molecular potentials. In *International Conference on Learning Representations*, 2022.

[2] Yusong Wang, Shaoning Li, Xinheng He, Mingyu Li, Zun Wang, Nanning Zheng, Bin Shao, Tong Wang, and Tie-Yan Liu. ViSNet: a scalable and accurate geometric deep learning potential for molecular dynamics simulation. *Preprint at* `http://arxiv.org/abs/2210.16518`, 2022.

[3] Lars Ruddigkeit, Ruud Van Deursen, Lorenz C Blum, and Jean-Louis Reymond. Enumeration of 166 billion organic small molecules in the chemical universe database GDB-17. *J. Chem. Inf. Model.*, 52(11):2864–2875, 2012.

[4] Raghunathan Ramakrishnan, Pavlo O Dral, Matthias Rupp, and O Anatole Von Lilienfeld. Quantum chemistry structures and properties of 134 kilo molecules. *Sci. Data*, 1(1):1–7, 2014.

[5] Albert Musaelian, Simon Batzner, Anders Johansson, Lixin Sun, Cameron J Owen, Mordechai Kornbluth, and Boris Kozinsky. Learning local equivariant representations for large-scale atomistic dynamics. *Nat. Commun.*, 14(1):579, 2023.

[6] Yi-Lun Liao and Tess Smidt. Equiformer: Equivariant graph attention transformer for 3D atomistic graphs. In *The Eleventh International Conference on Learning Representations*, 2023.

[7] Yang You, Jing Li, Sashank Reddi, Jonathan Hseu, Sanjiv Kumar, Srinadh Bhojanapalli, Xiaodan Song, James Demmel, Kurt Keutzer, and Cho-Jui Hsieh. Large batch optimization for deep learning: Training bert in 76 minutes. In *International Conference on Learning Representations*, 2020.

[8] Ask Hjorth Larsen, Jens Jørgen Mortensen, Jakob Blomqvist, Ivano E Castelli, Rune Christensen, Marcin Dułak, Jesper Friis, Michael N Groves, Bjørk Hammer, Cory Hargus, et al. The atomic simulation environment—a python library for working with atoms. *J. Condens. Matter Phys.*, 29(27):273002, 2017.

[9] Xiang Fu, Zhenghao Wu, Wujie Wang, Tian Xie, Sinan Keten, Rafael Gomez-Bombarelli, and Tommi S Jaakkola. Forces are not enough: Benchmark and critical evaluation for machine learning force fields with molecular simulations. *Transactions on Machine Learning Research*, 2023.